Supplementary materials

The organic ammonium counterion effect on slow magnetic relaxation of the [Er(hfac)₄]⁻ complexes

Tatiana G. Prokhorova, Denis V. Korchagin *, Gennady V. Shilov, Aleksei I. Dmitriev, Mikhail V. Zhidkov and Eduard B. Yagubskii *

Federal Research Center of Problems of Chemical Physics and Medicinal Chemistry, Russian Academy of Sciences, 142432 Chernogolovka, Russian Federation
* Correspondence: authors E-mail addresses: korden@icp.ac.ru (D.V.K.); yagubski@gmail.com (E.B.Y.)

Table S1. Selected bond lengths [Å] and angles [deg] for **5**.

Er(1)-O(1)	2.308(3)	Er(2)-O(9)	2.299(3)	Er(3)-O(17)	2.306(3)
Er(1)-O(4)	2.311(3)	Er(2)-O(12)	2.316(3)	Er(3)-O(19)	2.309(3)
Er(1)-O(8)	2.312(3)	Er(2)-O(14)	2.316(3)	Er(3)-O(23)	2.318(3)
Er(1)-O(6)	2.322(3)	Er(2)-O(10)	2.319(3)	Er(3)-O(21)	2.322(3)
Er(1)-O(5)	2.325(3)	Er(2)-O(11)	2.320(3)	Er(3)-O(20)	2.322(3)
Er(1)-O(2)	2.327(3)	Er(2)-O(16)	2.322(3)	Er(3)-O(18)	2.327(3)
Er(1)-O(7)	2.328(3)	Er(2)-O(13)	2.331(3)	Er(3)-O(22)	2.329(3)
Er(1)-O(3)	2.330(3)	Er(2)-O(15)	2.334(3)	Er(3)-O(24)	2.339(3)
O(1)-Er(1)-O(4)	80.12(10)	O(9)-Er(2)-O(12)	112.62(9)	O(17)-Er(3)-O(19)	113.58(10)
O(1)-Er(1)-O(8)	73.79(10)	O(9)-Er(2)-O(14)	72.88(11)	O(17)-Er(3)-O(23)	137.93(10)
O(4)-Er(1)-O(8)	148.41(10)	O(12)-Er(2)-O(14)	74.66(10)	O(19)-Er(3)-O(23)	81.56(10)
O(1)-Er(1)-O(6)	113.28(9)	O(9)-Er(2)-O(10)	75.22(10)	O(17)-Er(3)-O(21)	75.21(10)
O(4)-Er(1)-O(6)	137.49(10)	O(12)-Er(2)-O(10)	149.66(10)	O(19)-Er(3)-O(21)	73.14(10)
O(8)-Er(1)-O(6)	70.92(10)	O(14)-Er(2)-O(10)	80.43(10)	O(23)-Er(3)-O(21)	145.37(10)
O(1)-Er(1)-O(5)	149.01(10)	O(9)-Er(2)-O(11)	145.35(11)	O(17)-Er(3)-O(20)	148.63(10)
O(4)-Er(1)-O(5)	76.02(10)	O(12)-Er(2)-O(11)	74.83(9)	O(19)-Er(3)-O(20)	75.82(10)
O(8)-Er(1)-O(5)	134.25(10)	O(14)-Er(2)-O(11)	139.01(10)	O(23)-Er(3)-O(20)	71.34(10)
O(6)-Er(1)-O(5)	74.02(9)	O(10)-Er(2)-O(11)	116.26(9)	O(21)-Er(3)-O(20)	79.69(10)
O(1)-Er(1)-O(2)	74.39(9)	O(9)-Er(2)-O(16)	82.56(10)	O(17)-Er(3)-O(18)	75.01(10)
O(4)-Er(1)-O(2)	72.57(10)	O(12)-Er(2)-O(16)	135.36(10)	O(19)-Er(3)-O(18)	145.59(11)
O(8)-Er(1)-O(2)	83.37(10)	O(14)-Er(2)-O(16)	147.87(10)	O(23)-Er(3)-O(18)	72.51(10)
O(6)-Er(1)-O(2)	148.75(10)	O(10)-Er(2)-O(16)	73.39(10)	O(21)-Er(3)-O(18)	139.13(10)
O(5)-Er(1)-O(2)	115.88(9)	O(11)-Er(2)-O(16)	71.13(10)	O(20)-Er(3)-O(18)	115.04(10)
O(1)-Er(1)-O(7)	136.77(10)	O(9)-Er(2)-O(13)	139.91(10)	O(17)-Er(3)-O(22)	78.97(10)
O(4)-Er(1)-O(7)	115.35(9)	O(12)-Er(2)-O(13)	78.97(10)	O(19)-Er(3)-O(22)	140.53(10)
O(8)-Er(1)-O(7)	74.99(10)	O(14)-Er(2)-O(13)	73.92(10)	O(23)-Er(3)-O(22)	114.97(10)
O(6)-Er(1)-O(7)	83.18(10)	O(10)-Er(2)-O(13)	77.69(10)	O(21)-Er(3)-O(22)	74.70(9)
O(5)-Er(1)-O(7)	72.50(10)	O(11)-Er(2)-O(13)	73.90(10)	O(20)-Er(3)-O(22)	76.47(10)
O(2)-Er(1)-O(7)	72.98(10)	O(16)-Er(2)-O(13)	116.97(10)	O(18)-Er(3)-O(22)	72.64(10)
O(1)-Er(1)-O(3)	71.93(10)	O(9)-Er(2)-O(15)	70.11(10)	O(17)-Er(3)-O(24)	74.07(10)
O(4)-Er(1)-O(3)	74.61(9)	O(12)-Er(2)-O(15)	72.17(10)	O(19)-Er(3)-O(24)	71.12(10)
O(8)-Er(1)-O(3)	112.62(9)	O(14)-Er(2)-O(15)	114.07(9)	O(23)-Er(3)-O(24)	74.77(10)
O(6)-Er(1)-O(3)	72.33(10)	O(10)-Er(2)-O(15)	135.26(10)	O(21)-Er(3)-O(24)	116.97(10)

O(5)-Er(1)-O(3) 82.79(10)	O(11)-Er(2)-O(15) 81.29(10)	O(20)-Er(3)-O(24) 135.32(10)
O(2)-Er(1)-O(3) 136.10(10)	O(16)-Er(2)-O(15) 74.86(10)	O(18)-Er(3)-O(24) 80.36(10)
O(7)-Er(1)-O(3) 149.19(10)	O(13)-Er(2)-O(15) 145.93(10)	O(22)-Er(3)-O(24) 145.85(10)

Table S2. Shape analysis for different Er(III) ions in **5**.

Structure [ErO$_8$]	OP-8	HPY-8	HBPY-8	CU-8	SAPR-8	TDD-8	JGBF-8
Er1	29.782	23.289	14.734	7.253	0.497	2.108	15.967
Er2	29.098	23.587	14.857	8.051	0.361	2.197	15.244
Er3	28.912	23.542	15.354	8.447	0.273	2.061	15.479

Table S2. (continuation)

Structure [ErO$_8$]	JETBPY-8	JBTP-8	BTPR-8	JSD-8	TT-8	ETBPY-8
Er1	29.171	3.231	2.543	5.527	8.069	23.825
Er2	28.182	2.966	2.322	5.391	8.893	23.351
Er3	28.457	2.800	2.271	5.106	9.248	23.671

OP-8 Octagon (*D$_{8h}$*) , **HPY-8** Heptagonal pyramid (*C$_{7v}$*), **HBPY-8** Hexagonal bipyramid (*D$_{6h}$*), **CU-8** Cube (*O$_h$*), **SAPR-8** Square antiprism (*D$_{4d}$*), **TDD-8** Triangular dodecahedron (*D$_{2d}$*), **JGBF-8** Johnson-Gyrobifastigium (J26) (*D$_{2d}$*), **JETBPY-8** Johnson-Elongated triangular bipyramid (J14) (*D$_{3h}$*), **JBTP-8** Johnson- Biaugmented trigonal prism (J50) (*C$_{2v}$*), **BTPR-8** Biaugmented trigonal prism (*C$_{2v}$*), **JSD-8** Snub disphenoid (J84) (*D$_{2d}$*), **TT-8** Triakis tetrahedron (*T$_d$*)**, ETBPY-8** Elongated trigonal bipyramid (*D$_{3h}$*).

Table S3. The shortest intermolecular contacts.

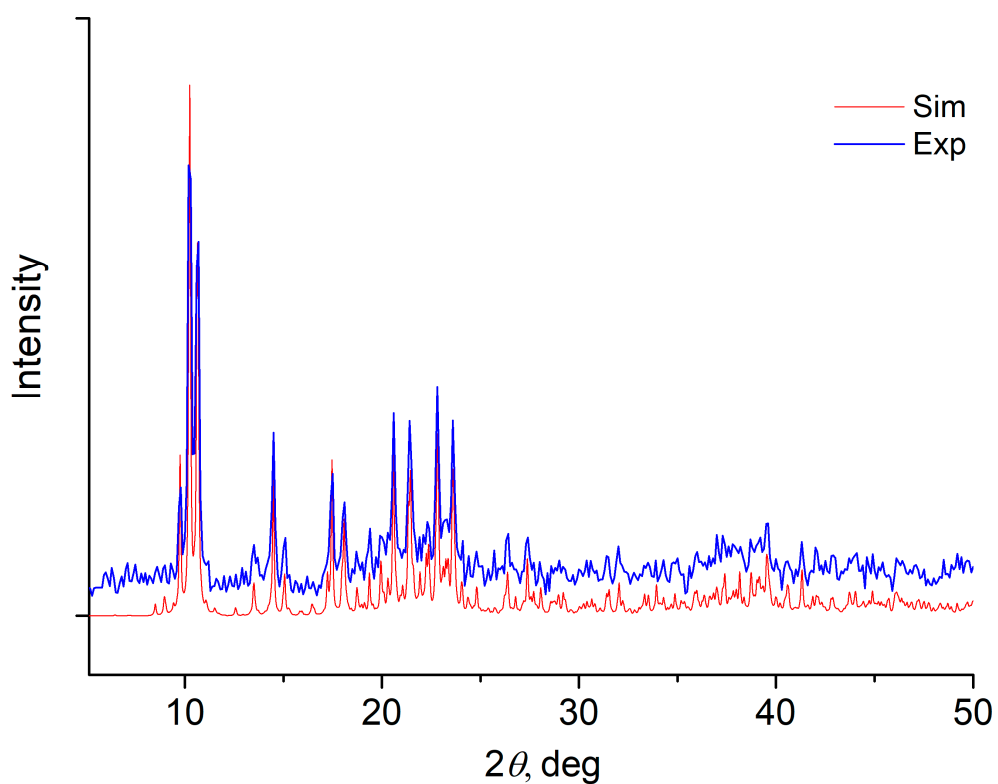| Atom1	Atom2	d,Å		Atom1	Atom2	d,Å
F13	F100	2.925		F22	C175	3.116
F24	F44	2.874		F12	C151	2.998
C16	F26	3.137		O1	C174	3.129
F8	F39	2.894		O8	C174	3.179
F18	F36	2.931		F146	F32	2.905
C8	F62	3.137		F35	F36	2.929
F10	F49	2.911		C31	F60	3.155
F4	F47	2.802		F26	F55	2.677
F2	F70	2.868		F38	F63	2.905
F2	F64	2.859		F28	C184	3.120
F13	C173	3.141		F179	C177	3.152

Figure S1. Experimental (blue) and simulated from single-crystal data (red) powder X-ray diffraction pattern of polycrystalline sample of **5**.
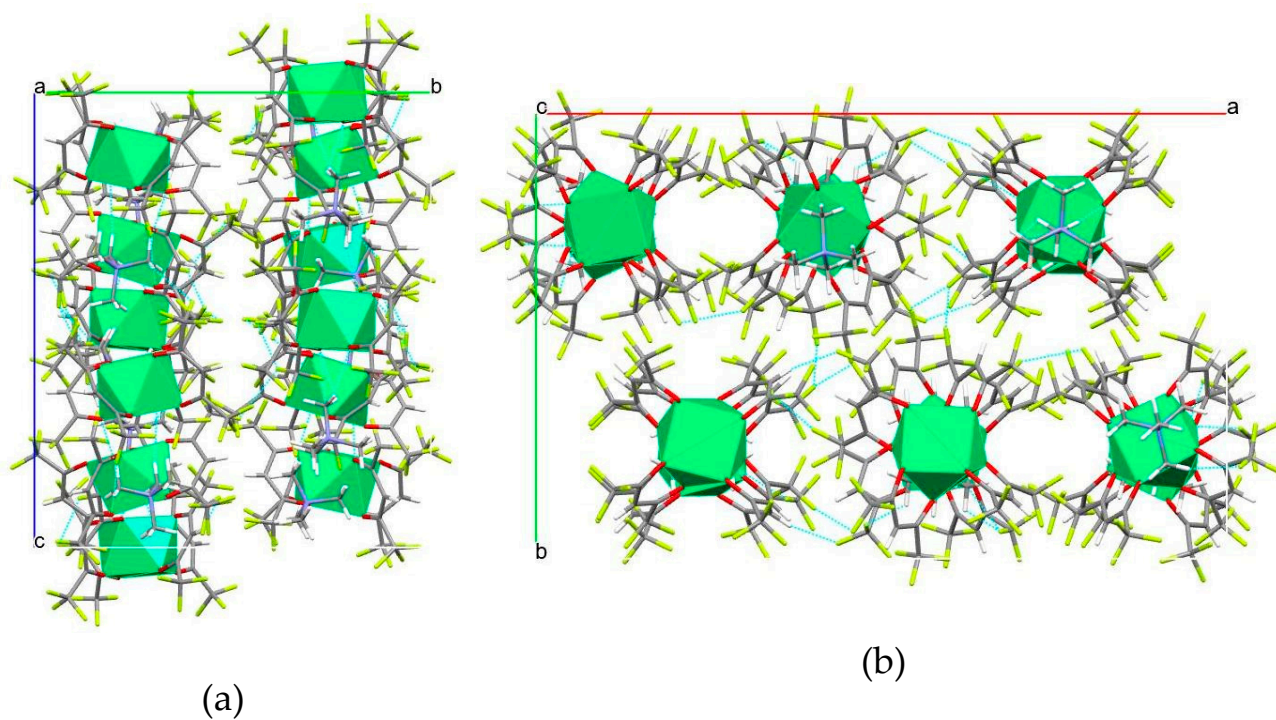

(a)

(b)

Figure S2. Projections of the fragments of the crystal structure of **5** on *bc* and *ab* crystallographic planes. Dashed cyan lines show shortest intermolecular contacts.
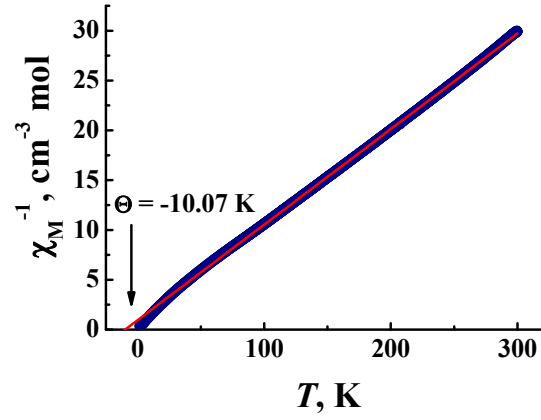
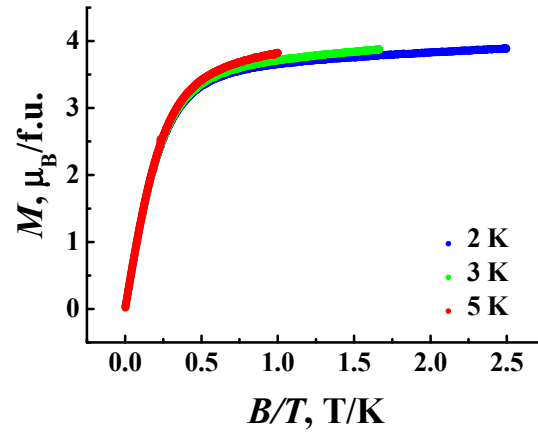**Figure. S3.** Plot of the $1/\chi_M$ vs T. The red solid line represents the extrapolation of the high-temperature data to $1/\chi_M = 0$. The arrow marks the Weiss temperature.

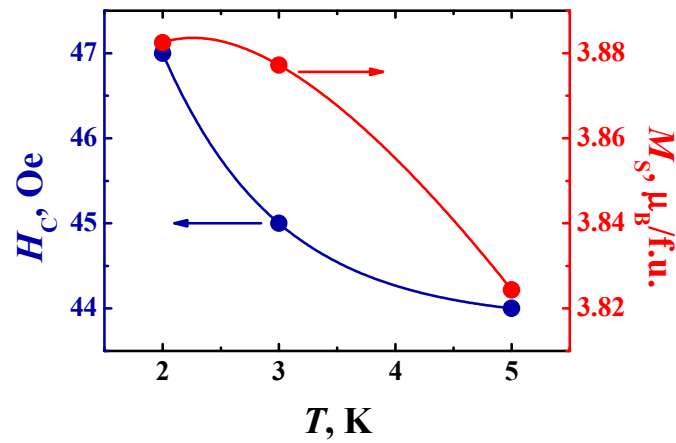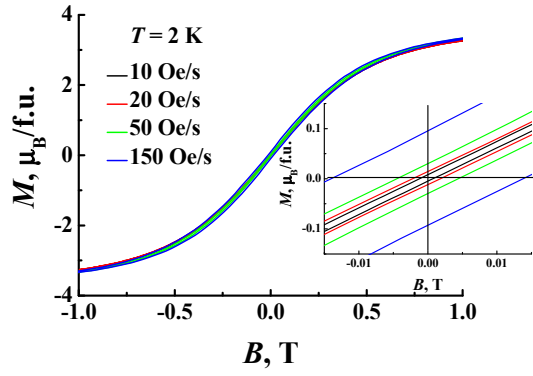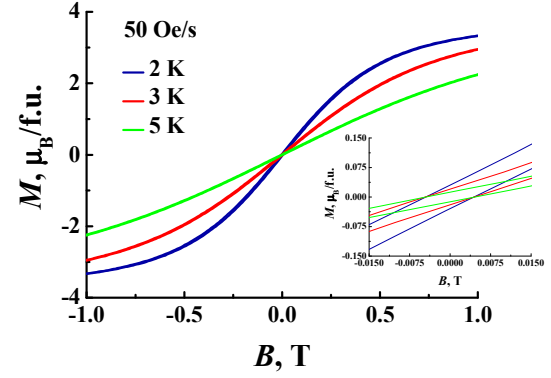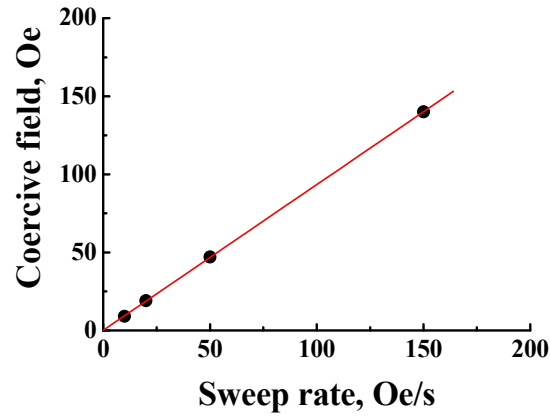**Figure S4.** M vs BT^{-1} plots at 2, 3 and 5 K.

Figure S5. Temperature dependences of the saturation magnetization and coercive field. The solid lines show the splines.

(**a**)

(**b**)

c)

Figure S6. Hysteresis loops at different magnetic field sweep rates (a) and temperatures (b). The inset shows low-field fragments of loops. c) Dependence of the coercive field on the magnetic field sweep rate at a temperature of 2 K.
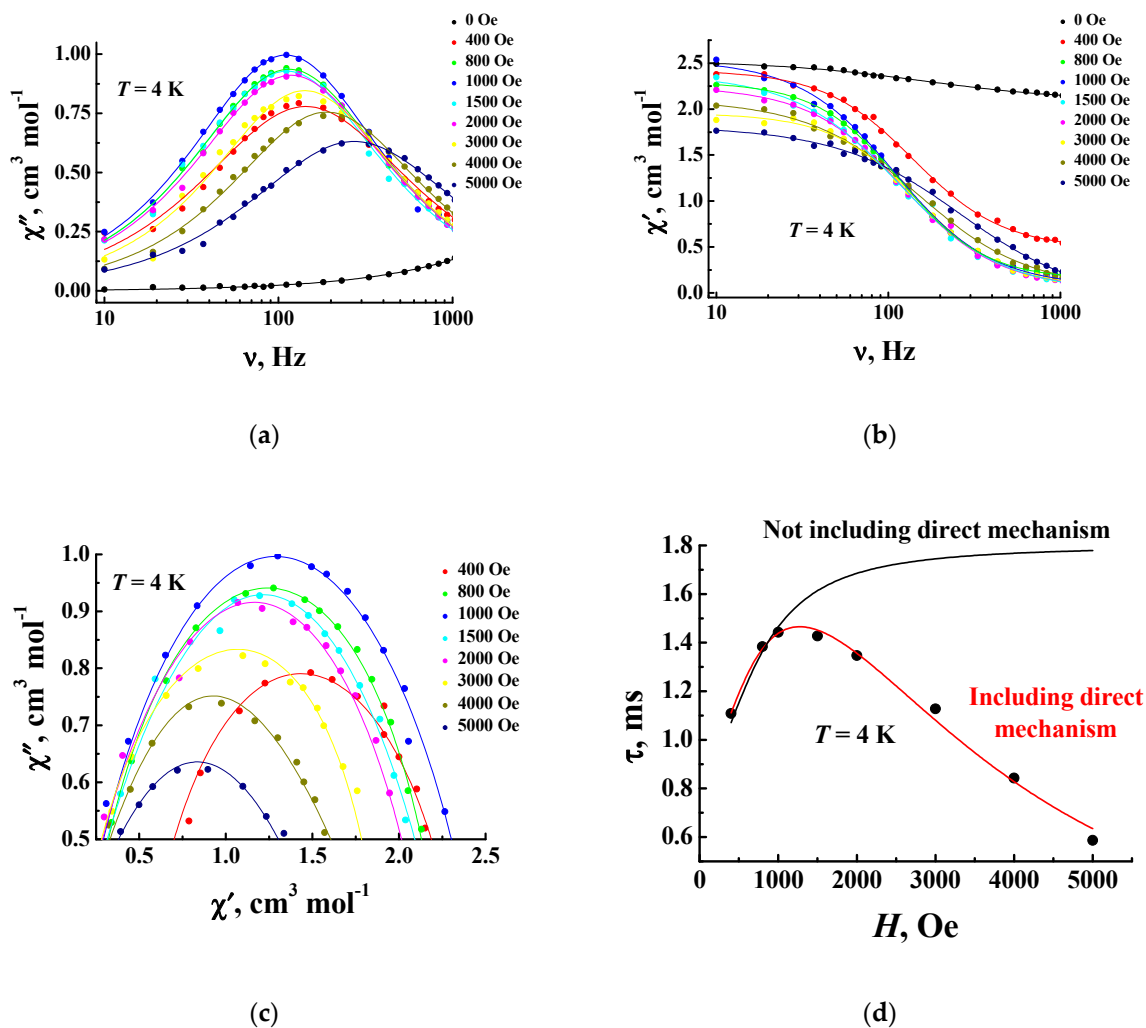
(a)

(b)

(c)

(d)

Figure S7. Frequency dependences of the in-phase (a) and out-of-phase (b) ac susceptibility; (c) Cole-Cole plots for complex **5** at 4 K and indicated dc fields; (d) field dependence of the relaxation time τ at 4 K. Symbols are experimental data, solid lines indicate fits.

Table S4. Fit parameters for **5** at 4 K and indicated dc fields (R^2 = 0.99913).

H, Oe	χ_S, cm^3 mol^{-1}	$\Delta\chi_T$, cm^3 mol^{-1}	τ, s	α
400	0.470	1.861	$1.108 \cdot 10^{-3}$	0.103
800	0.135	2.102	$1.383 \cdot 10^{-3}$	0.071
1000	0.052	2.248	$1.442 \cdot 10^{-3}$	0.076
1500	0.044	2.074	$1.426 \cdot 10^{-3}$	0.070
2000	0.029	2.048	$1.347 \cdot 10^{-3}$	0.071
3000	0.054	1.898	$1.127 \cdot 10^{-3}$	0.082
4000	0.019	1.711	$0.842 \cdot 10^{-3}$	0.082
5000	0.010	1.533	$0.585 \cdot 10^{-3}$	0.118

Table S5. Fit parameters for **5** at 1000 Oe dc fields and indicated temperatures (R^2 = 0.99968).

T, K	χ_S, cm³ mol⁻¹	$\Delta\chi_T$, cm³ mol⁻¹	τ, s	α
3	0.091	2.688	$8.624 \cdot 10^{-3}$	0.119
3.5	0.078	2.251	$3.073 \cdot 10^{-3}$	0.064
4	0.052	2.248	$1.442 \cdot 10^{-3}$	0.076
4.5	0.090	1.738	$0.724 \cdot 10^{-3}$	0.075
5	0.062	1.518	$0.415 \cdot 10^{-3}$	0.089
5.5	0.037	1.365	$0.257 \cdot 10^{-3}$	0.068
6	0.036	1.225	$0.171 \cdot 10^{-3}$	0.067
6.5	0.034	1.135	$0.116 \cdot 10^{-3}$	0.074
7	0.035	1.063	$0.085 \cdot 10^{-3}$	0.069
7.5	0.032	0.981	$0.065 \cdot 10^{-3}$	0.074
8	0.030	0.914	$0.047 \cdot 10^{-3}$	0.088
8.5	0.028	0.816	$0.041 \cdot 10^{-3}$	0.067
9	0.027	0.763	$0.031 \cdot 10^{-3}$	0.076
9.5	0.024	0.676	$0.028 \cdot 10^{-3}$	0.059
10	0.023	0.681	$0.020 \cdot 10^{-3}$	0.083